Traffic equations and granular convection

Daniel C. Hong* and Su Yue†

Department of Physics, Lewis Laboratory, Lehigh University, Bethlehem, Pennsylvania 18015

(Received 24 March 1998)

We investigate both numerically and analytically the convective instability of granular materials by two-dimensional traffic equations. In the absence of vibrations traffic equations assume two distinctive classes of fixed bed solutions with either a spatially uniform or nonuniform density profile. The former one exists only when the function $V(\rho)$ that monitors the relaxation of grains assumes a cutoff at the closed packed density, ρ_c, with $V(\rho_c)=0$, while the latter one exists for any form of V. Since there is little difference between the uniform and nonuniform solution deep inside the bed, the convective instability of the bulk may be studied by focusing on the stability of the uniform solution. In the presence of vibrations, we find that the uniform solution bifurcates into a bouncing solution, which then undergoes a supercritical bifurcation to the convective instability. We determine the onset of convection as a function of control parameters and confirm this picture by solving the traffic equations numerically, which reveals bouncing solutions, two convective rolls, and four convective rolls. Further, convective patterns change as the aspect ratio changes: in a vertically long container, the rolls move toward the surface, and in a horizontally long container, the rolls move toward the side walls. We compare these results with the those reported previously with a different continuum model by Hayakawa, Yue, and Hong [Phys. Rev. Lett. **75**, 2328 (1995)]. Finally, we also present a derivation of the traffic equations from Enskoq equation. [S1063-651X(98)09410-0]

PACS number(s): 81.05.Rm, 47.20.−k, 46.10.+z

I. INTRODUCTION

This paper is concerned with the numerical as well as the analytical analysis of two-dimensional traffic equations, termed model B in the literature [1] with an aim to understand the convective instability of granular materials. It has been known since Faraday [2] that the granular materials in a vibrating bed develop permanent convective rolls when the strength of the vibration exceeds a critical value. Unlike the well known Rayleigh-Bénard thermal convection in fluids, however, the origin of the granular convection has remained relatively unexplored since its discovery, but recently two simultaneous works from the experimental side [3,4] with the use of a MRI or x-ray method as well as from computer simulations based on the distinct element method [5] have substantially aided our understanding through visualization. Yet, the theoretical efforts to uncover the basic mechanism of this granular convection have not been remarkable, still largely focused on producing convective patterns through computer models and simulations. While much impressive experimental data are currently being piled up, theoretical development [6–10] in this area seems to be still far from complete. In order to have a deeper understanding of the granular convection, we find it essential to come up with a reasonable continuum model that contains a minimum number of control parameters yet captures some of the essence of granular convection. The goal is certainly to explore analytically and numerically the instability mechanisms that lead to many fascinating complex nonlinear dynamics behaviors.

Our aim here is twofold: We first present such a continuum model along with previously unpublished numerical

results based on two-dimensional traffic equations, and second, we carry out the linear stability analysis of the traffic equations and uncover the mechanism of granular convection as a supercritical bifurcation of a bouncing solution. This mechanism for the granular convection is essentially identical to the previously obtained scenario for a different continuum model, termed model A [8]. However, detailed simulations of these two continuum models reveal distinctively different convection patterns for different geometries and parameter ranges. The most notable departure between the two is the migration of convective rolls toward the surface and toward the walls in model B, as the aspect ratio changes. This is in sharp contrast with the results of model A, which predict a series of rolls in the container. Further, the simulation results of model B yield rich dynamical behaviors as we probe deeper into the parameter space, yet the analytical structure of the nontrivial patterns seems to be quite complex and requires further extensive studies in the future. Our analytical study here focuses exclusively on the stability analysis of a uniform bouncing solution, but there exists a second class of solutions that are spatially nonuniform. The stability analysis of the latter is highly nontrivial and we only present a brief description of it in Appendix B. Fortunately, however, since there is little difference between the uniform and nonuniform solutions deep inside the bed, we expect that the uniform bouncing solution may capture the essence of the bulk instability. For details, see the text.

This paper is organized as follows. We first define the model equations in Sec. II and make an attempt to derive the traffic equations from the Enskog equation in Appendix A. We will then present numerical results in Sec. II, and provide some insight into the stability mechanism of the granular convection in Sec. III. We also discuss several unresolved questions in Sec. IV. We now turn to the main text.

*Electronic address: dh09@lehigh.edu
†Electronic address: sufrank.yue@citicorp.com

II. TWO-DIMENSIONAL TRAFFIC EQUATIONS AND GRANULAR CONVECTION

Apart from its wide application to traffic flow problems [12], the traffic equations [13–15] have recently been proposed as an alternative continuum model to the Navier-Stokes equation, in investigating a variety of dynamical responses of granular materials. Examples include the granular relaxation under repeated tapping [16], density waves and jamming and clogging phenomena [11,14,17], $1/f$ spectrum of hopper flow [18], and granular segregation [19]. But we point out that, unlike the studies to be presented in this paper, almost all of the studies thus far have focused exclusively on *one*-dimensional traffic equations [13–19], which certainly will not be able to describe the granular convection. Hence, we first present here the two-dimensional version of the traffic equations [1], termed model B in Ref. [1]:

$$\frac{\partial \rho}{\partial t} + \frac{\partial \rho v_x}{\partial x} + \frac{\partial \rho v_z}{\partial z} = 0, \qquad (1)$$

$$\frac{\partial v_x}{\partial t} + v_x \frac{\partial v_x}{\partial x} + v_z \frac{\partial v_x}{\partial z} = -c_0^2/\rho \frac{\partial \rho}{\partial x} + \mu\left(\frac{\partial^2 v_x}{\partial x^2} + \frac{\partial^2 v_x}{\partial z^2}\right), \qquad (2)$$

$$\frac{\partial v_z}{\partial t} + v_z \frac{\partial v_z}{\partial z} + v_x \frac{\partial v_z}{\partial x} = \frac{V(\rho,t) - v_z}{\tau} - c_0^2/\rho \frac{\partial \rho}{\partial z}$$
$$+ \mu\left(\frac{\partial^2 v_z}{\partial x^2} + \frac{\partial^2 v_z}{\partial z^2}\right), \qquad (3)$$

where $c_0^2 \sim T_e$ is the sound speed, and μ is the viscosity. One may add $-v_x/\tau$ on the right-hand side of Eq. (2). Before proceeding further, we point out some of the conceptual problems associated with the traffic equations. First of all, the momentum equation in the conventional Navier-Stokes equation is written as

$$dv_i/dt = -\partial_{ij}\sigma_j + F_i,$$

where d/dt is the total derivative, and σ_{ij} is the stress tensor representing all the internal forces, and F_i is the external force imposed on the system. The reason the internal forces are written as a divergence is because of the momentum conservation and the total sum of the volume force must vanish because of Newton's third law. Further, since the volume integral of the divergence can be replaced by the surface integral, we must impose the boundary condition that the normal component of the stress tensor vanishes at the surface. On the other hand, in the traffic equations the momentum equations, (2) and (3), are not written this way, and this may call for questions in utilizing the traffic equations in granular convection. In the presence of interstitial fluids such as air, the use of traffic equations may be justified in the sense that the relaxation term may be effectively equivalent to assuming a drag force as was done in Appendix A. However, in the absence of air, justification of the drag term is difficult and our conjecture, which has yet to be proven, is that the long range correlations among voids may produce a term that is not written as the divergence. To be more specific, we point out that the difference between model B [1] and model A [8] is the presence of the relaxation term in the

z direction, which is represented by an average function $V(\rho,t)$ with the relaxation time τ. The net effect is for the void (or particle) to adjust its speed, v_z, around the average value $V(\rho)$ in a given time τ. The origin of such a term has been discussed by Hong *et al.* [16] in an attempt to introduce correlations among grains or voids in the diffusing void model (DVM) [20]. In the DVM, the void speed is only a function of local void density, namely, $v_z = V(\rho)$ + diffusion term. However, a void is a compressible hydrodynamic object that changes and adjusts its shape to conform to the surroundings, not instantaneously, but in a given finite time τ. So, it may be more appropriate to write down the time-dependent equation for the velocity in a manner given by Eq. (3) than to simply assume a fixed value at a given local density. The presence of such a relaxation process may be effectively equivalent to assuming a drag force acting on a void, which is reasonable if there is interstitial fluid such as air. In the absence of interstitial fluid, the only reasonable conclusion is to assume that its origin lies in the frictions of the front and the rear glass of the container and from the wall.

The coupled equations (1)–(3) are fairly similar to the two-phase model [26] of a fluidized bed that has been widely used for mixtures of gas and granular particles. As shown in Appendix A, functions in the traffic equations (1)–(3) may be inferred from the Enskog equation [21]; namely, $-v_z/\tau$ is the drag term imposed externally on the particle, or by vibrations. Further, the Enskog pressure, $T\rho[1+f(\rho)\rho/2]$ with $f(\rho)$ the correlation function, produces an extra term $V(\rho)$ in addition to the hard sphere pressure $T\rho$. In this case, we make an important observation that the coefficient of $V(\rho)$ is proportional to the gravity g, which will enable us to incorporate the vibrations of the bed. This observation makes sense, because the strength of the mean speed (also termed the drift velocity) is determined by the gravity and thus it is quite physical to assume that the mean speed of the void is also proportional to the gravity as demonstrated in [16] and Appendix A. In the moving frame of reference of the vibrating bed, the mean speed $V(\rho)$ depends not only on the density but also on the way the box is shaken. In the moving frame, the effective gravity, $g' = -g + A\omega^2\cos(\omega t)$, is the only time-dependent factor involved in the mean speed $V(\rho)$. Therefore, without the loss of generality, we expect that the mean speed of the granular flow along the z direction assumes the following form:

$$V(\rho) = V_0(\rho)g' = V_0'(\rho)[-1 + \Gamma \sin(\omega t)], \qquad (4)$$

where $\Gamma = A\omega^2/g$ with A the amplitude of the vibration, and ω the vibrational frequency. $V_0(\rho)$ is the mean speed in the absence of the vibration, such as the case in the hopper flow. In one-dimensional traffic equation, we have used [16]:

$$V_0(\rho) = \alpha/(1 + \beta\rho^2). \qquad (5)$$

Note that the functional form of V_0 is not unique, and other exponentially decaying functions have also been proposed [13]. The $V_0(\rho)$ assumed above has a long tail when the density increases, which might be unphysical since there should be a critical density, ρ_c, for any granular material, at which all particles will be locked in if the density exceeds that critical density. This critical density may be proportional
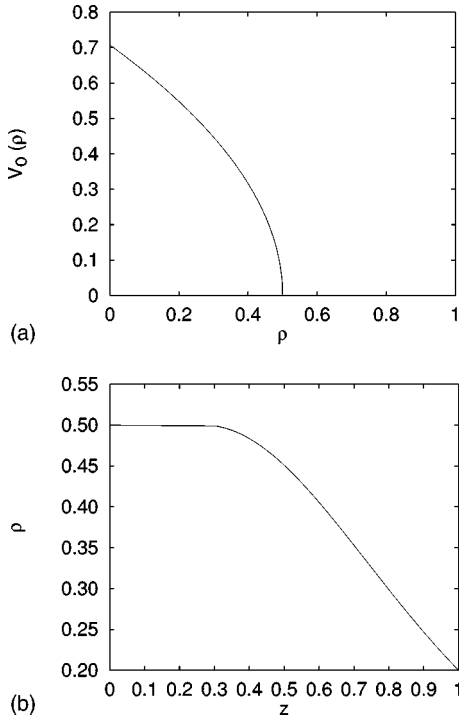
FIG. 1. (a) Mean speed $V_0(\rho)$ as a function of density is plotted above (a), with the cutoff density $\rho_c = 0.501$ and $\beta = 1/2$. (b) Static solution is solved analytically and the density ρ is plotted as a function of the height z, where $z = 0$ is the bottom of the container. The numerically obtained result solution of Eqs. (1)–(3) is consistent with this up to a very high accuracy.

or equal to the closed packed density. Thus, we have employed a different form in our numerical simulations that assume the form [Fig. 1(a)]:

$$V(\rho) = (\rho_c - \rho)^\beta \theta(\rho_c - \rho), \qquad (6)$$

where we have used a step function $\theta(\rho_c - \rho) = 0$ when $\rho \geq \rho_c$. A physically reasonable choice of β may be such that $V'(\rho) < \infty$. [For $\beta < 1$, $V'(\rho)$ diverges at ρ_c, and thus in our stability criterion, we set the density of the uniform solution slightly less than the closed packed density.] Before investigating Eqs. (1)–(3) numerically, we first check the consistency.

A. Consistency check: static solutions without vibrations

It is worthwhile to examine a few special cases not only for the sake of general limitation, but also to check the numerical accuracy. When $\Gamma = A\omega^2/g = 0$, which corresponds to the case without the vibration, which we also term ''the fixed bed solution,'' we expect a static solution where $\vec{v} = 0$ in all momentum equations. We note that there are *two* classes of static solutions.

First, we discuss a spatially nonuniform solution. Regardless of the functional form of $V(\rho)$, we find by inspection that there exists a spatially nonuniform static solution that satisfies the following differential equation:

$$V_0(\rho) = \frac{c_0}{\rho} \nabla \rho. \qquad (7)$$

This represents a situation where particles pile up from the top to bottom with a certain density distribution. For simplicity, the mean speed is assumed to satisfy Eq. (6). The mean speed as a function of density is plotted in Fig. 1(a). When the density of the granular particles exceeds the critical density, say, for example, $\rho_c = 0.501$, the particles become locked and have a steady-state density $\rho = \rho_c$. If we solve Eq. (7) and plot the density profile as a function of z [Fig. 1(b)], we can see that the uniform density profile is created close to the bottom of the plate, and then the density decreases linearly to zero as we move to the top of the container. Physically, this is acceptable if we notice that when the particles near the bottom are locked, they act more like a solid. On the other hand, those particles near the surface are rather loosely packed and ready to move, which is more like a traditional fluid, where the density linearly decreases as the altitude increases. Note that the granular bed is not subjected to vibrations at this time and thus this is a fixed bed solution. Furthermore, the total number of particles is conserved by the mass conservation law of Eq. (1). The flat region in the density profile can be extended all the way to the surface by changing the exponent β. We emphasize that the nonslip fluid boundary conditions have been imposed at the top and bottom plates as well as at the side walls in solving the equations numerically, namely, $v_\perp = 0$ and $v_\parallel = 0$ [8].

Second, a spatially uniform solution. There is, however, a second class of solution that exists only when $V(\rho)$ has a cutoff. This solution is a spatially uniform solution with the density given by the closed packed density, ρ_c, everywhere with $V(\rho_c) = 0$. Numerical simulations of the traffic equations reveal that it is the spatially nonuniform solution that is realized in simulations. But the stability analysis of the uniform solution clearly shows that this solution is stable, too, and thus it must be realized with presumably suitable boundary conditions. Further, deep inside the bed, there is very little difference between the uniform and nonuniform solutions, and thus the convective instability inside the bulk may be investigated by focusing on the stability of the uniform bouncing solutions. In the absence of the rigorous stability analysis of the nonuniform solution, this is only our guess. Future work must focus on the rigorous stability analysis of the nonuniform solution (see Appendix B) and compare its result to those of the uniform solution obtained in Sec. III. Before presenting the stability analysis, we first present numerical results.

B. Numerical results

We now investigate the time-dependent phenomena numerically. Numerical solutions are obtained by two different algorithms for the rectangular boundaries. The first one is the center-difference method, which has the accuracy of second order in space and first order in time. The second method employed here is the Runge-Kutta algorithm, which has the accuracy of second order in space and third order in time. The results show that both methods give consistent conclusions for the same boundary conditions. For most of the cases, we set the grid number equal to $N_x = 32$ and $N_z = 32$ in order to improve the accuracy while accommodating the CPU cost. Lower or higher grid numbers have been examined as well, but no significant changes have been found.

Initially, the uniform solution is assumed, and typically four cycles are taken to calculate the average of the convection after the stable periodical solution appears at each site in the lattice. In the stream line plot, all of the vector flow arrows are normalized by the maximum speed. Numerically, we observe two distinctive classes of solutions: the first one is the bouncing solutions, and the second one the convective rolls. We first examine the bouncing solutions. Note that the set of parameters that correspond to physical situations might be $\omega/2\pi = 20$ Hz, $T_e \sim 3$, and $\mu = 1/R \approx 0.5$ with the Reynolds number $R = UL/\mu_s \approx 2$, because the kinetic viscosity of the granular material, $\mu_s \approx 5 \times 10^{-3}$ m^2/s and the typical velocity $U \approx 10$ cm/s [8]. For pure numerical reasons, however, in what follows, unless mentioned otherwise, all the simulations are conducted with the parameters, $\mu = 1, \omega = 1, \tau = 1$ and $T_e = 2, L = 32$ with $V_0(\rho)$ given by Fig. 1.

1. Bouncing solutions with $\Gamma \lesssim \Gamma_c$

For a fixed set of control parameters, bouncing solutions, first termed in [8], appear when the vibration strength Γ is less than the numerically determined critical value $\Gamma_c \approx 1.5$. Upon increasing Γ, this bouncing solution becomes unstable and bifurcates into a different branch and convective rolls appear. We have examined the case where the vibrational acceleration is less than the gravity, in other words, the dimensionless variable Γ is less than 1, which is certainly the regime below the critical strength. In real situations, for $\Gamma < 1$, nothing much really happens inside the box except perhaps the volume decreases due to settling caused by vibration. However, in our simulation, due to the presence of the top layer, which suppresses the complicated surface motions of the particles, we expect the bouncing solution to appear even for $\Gamma < 1$. We have performed the simulation using different initial conditions such as a uniform density distribution, a linear density distribution, or a fluctuation in the velocity field. For all cases, we have found that after a relatively long CPU time, the convection pattern disappears, which implies that the convection does not persist in this parameter regime. However, if we measure the local density or velocity at different locations, we clearly observe oscillatory solutions that persist everywhere inside the container. This is termed the "bouncing solution" that exists before the onset of the convection: the bulk of the granular material oscillates up and down, like a single solid ball, with a central frequency of the vibrating container and some harmonics. The harmonic oscillations of the density and velocity at the same lattice site are displayed in Figs. 2(a) and 2(b).

2. Convective domain with $\Gamma > \Gamma_c$

When $\Gamma > \Gamma_c$, the bouncing solutions disappear and the permanent convective rolls appear inside the bulk. In order to view this slow convection, we have to take the average of the velocity field over many periods. Typically four cycles are used, since the amplitude of the convection is relatively small in comparison to the amplitude of the vibration. This is true in experimental systems as well. In the stream-line plot, we have normalized the velocity field by taking the maximum velocity component as the maximum length of the arrows.
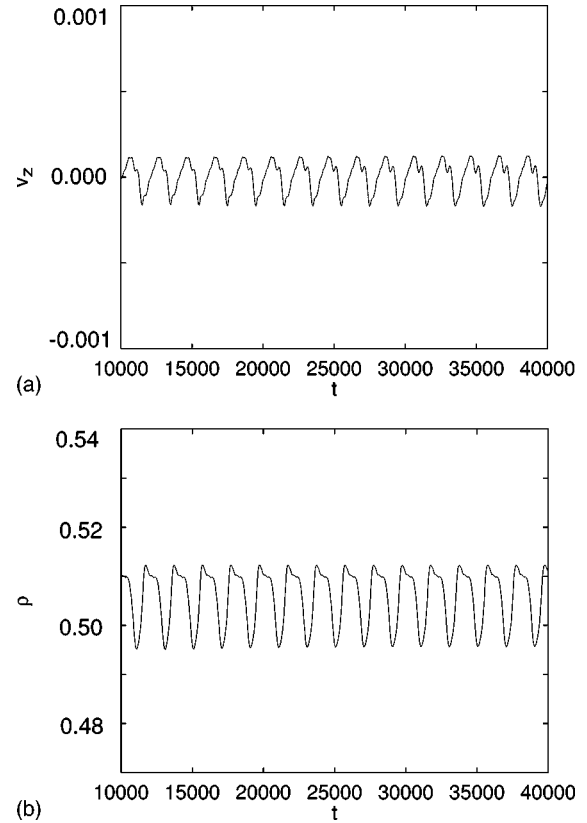

FIG. 2. Bouncing solutions for (a) the velocity v_z and (b) the density at the same fixed location $(x,z) = (15,15)$, where no convection rolls appear and the bulk of the particles moves as a single particle. $\Gamma < \Gamma_c$.

In Fig. 3(a) convection patterns are illustrated for $\Gamma = 2.25 > \Gamma_c$ by plotting the streamline of the velocity field, where $V_0 = (\rho_c - \rho)^\beta \theta(\rho_c - \rho)$ with $\beta = 2/3$ and $\rho_c = 0.501$ as given in Fig. 1, is used. Notice that the flow direction close to the wall is in the downward direction, and at the center of the container, the particles try to move up. [Note that the tail of the arrow is the direction of the flow, so the velocity profile is up at the center. The same applies for Figs. 6, 7, and 9.] The density profile is also plotted in Fig. 3(b), where the average of the density over one period remains close to the static solution. At any given time the density profile varies around such an average velocity.

Next, it has been found that the geometry plays an important role in the convection pattern formation [7,22] and we examine its effect on the convective instabilities. For example, the change of the aspect ratio [defined as (width)/(height)] may affect the relative position, the number of convection rolls, and the intensity of the convection with respect to the same vibration parameters. We have examined two particluar cases:

First, the numerical results displayed in Figs. 4(a) and 4(b) show that the location of the convection rolls migrate when the aspect ratio changes. For the aspect ratio, $N_x/N_z = 0.5$, convection rolls move toward the top of the container, and the particles close to the bottom are almost locked, allowing no relative motion to exist. This is consistent with the experiments and MD simulation results. Convection rolls are shown in Fig. 4(a) and the corresponding density profile is plotted in Fig. 4(b). Note that the stability analysis of model
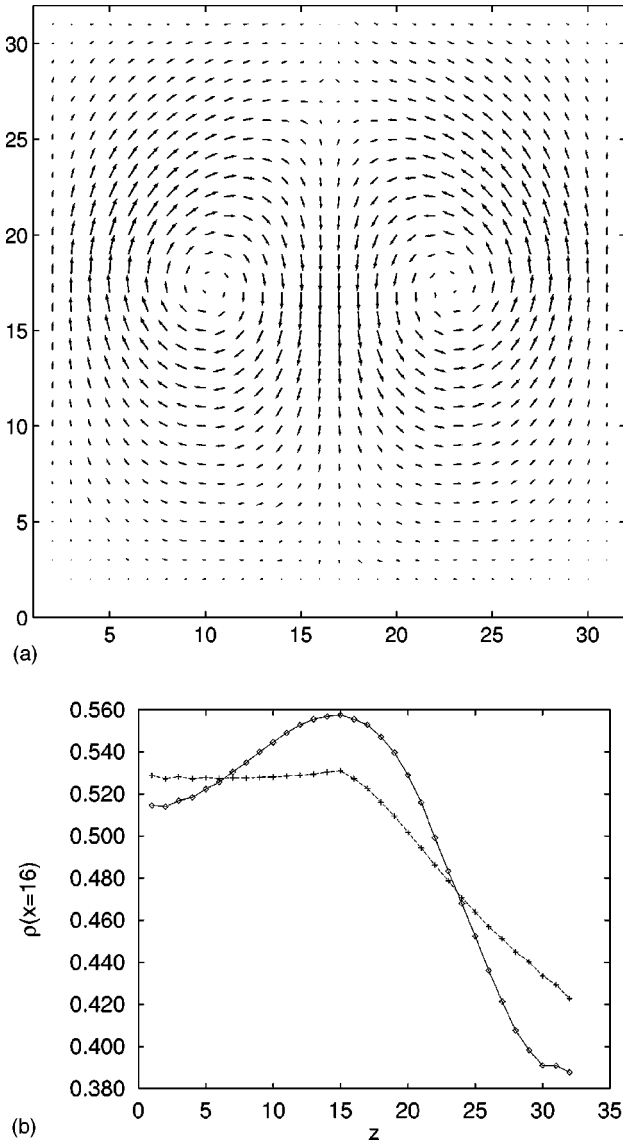
FIG. 3. Convection pattern and density profile: (a) When $\Gamma > \Gamma_c$, convection patterns are illustrated by plotting the streamline of the velocity field, where the velocity field is normalized by the maximum velocity component v_z, with V_0 given by Fig. 1. (b) The density profile as a function of position. The average of the density over one period remains close to the static solution $(+)$ and at any given time the density profile (circle) swings around such an average velocity.

A [8] predicts a series of rolls when the vertical axis increases as a multiple of the horizontal width. The form of $V(\rho)$ with a cutoff at the closed packed density seems to be crucial in capturing the real convective patterns. Further, the average density curve $(+)$ is very close to the static solution without the vibrations. The second curve $(-)$ is the density profile at the stop time t, which clearly shows that the density profile varies in time around the equilibrium density profile.

Second, we have also examined the case with the large aspect ratio, $N_x/N_z=2.0$ [results are shown in Fig. 5(a)], where the width is twice larger than the height. Here, four convection rolls appear with two small ones near the top corners [Fig. 5(a)]. If we extend the width even longer to the aspect ratio, $N_x/N_z=4$, the convection pattern will only exist
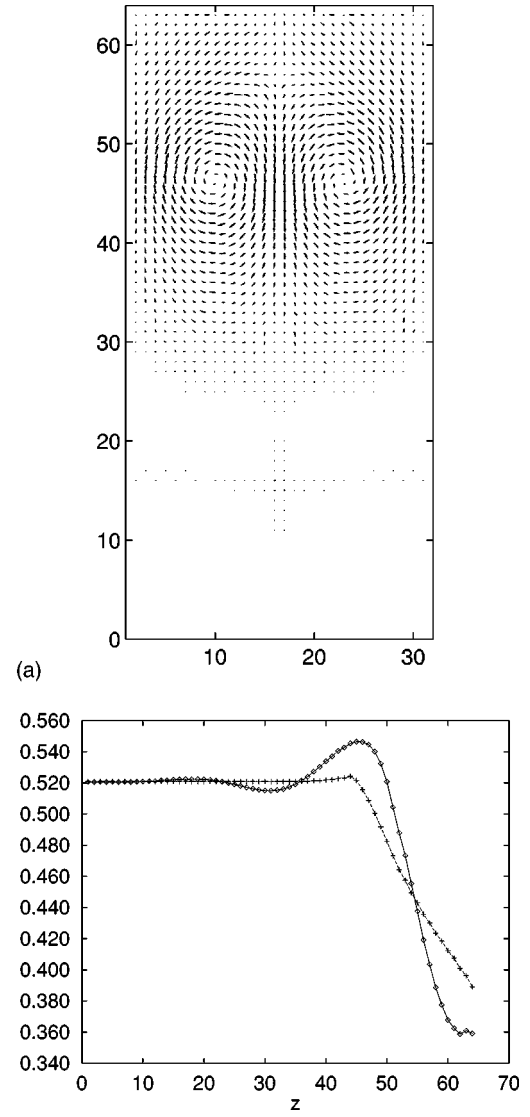
FIG. 4. Convection pattern for a small aspect ratio $N_x/N_z = 0.5$. All other parameters remain the same as in the case of $N_x/N_z=1.0$. (a) The two convection rolls move to the top region of the container and most of the particles close to the bottom are locked during the whole vibration cycles. This can be verified in the density profile at a fixed point $x=16$ (b), where the time-dependent density curve (circle) varies around the static solution (cross), but much less at the bottom than at the top regime.

around the narrow regime of side boundaries, represented by the zero intensity of convection [Fig. 5(b)]. It seems that convection rolls only appear close to the boundaries, which indicates that the friction on the wall presumably plays a significant role in the origin of the vibration-induced convections. Such observations are consistent with the observations made by Taguchi in molecular dynamics simulations [22].

3. Pattern dependence on $V_0(\rho)$

While we have not systematically examined the stability diagram of the many-dimensional parameter space, we report here a few cases simply to show the richness of the problem associated with the traffic equations. In the previous arguments, we have only assumed that $V_0(\rho)$ likely has a cutoff when the density exceeds a critical density (at which the
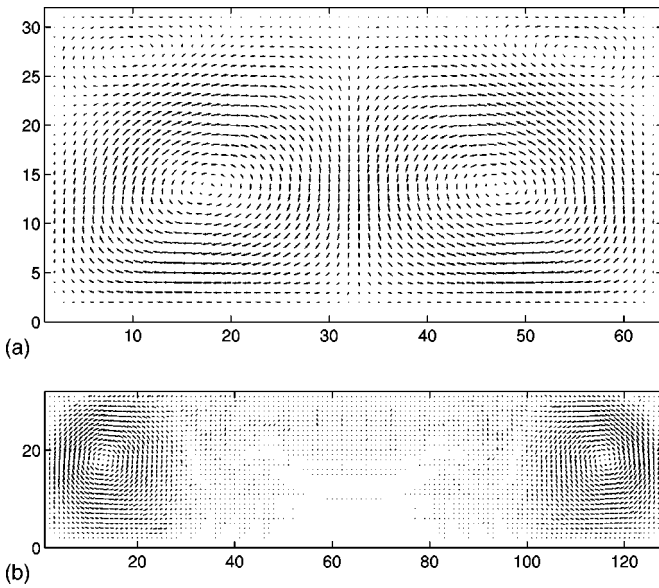
FIG. 5. Convection pattern for large geometry ratio. (a) Convection pattern is drawn for a large aspect tratio, $N_x/N_z = 2.0$. All other parameters remain the same as in the case of $N_x/N_z = 1.0$. Two main convection rolls appear at the center, with another two visible small convection rolls at the top corners of the container. The two small convection rolls have opposite spins relative to the major ones. (b) Two convective rolls for the aspect ratio $N_x/N_z = 4.0$ are illustrated for the same parameter regimes. The two rolls exist near the walls. They are separated by a wide nonconvection regime, where the velocity field equals zero.

particles become locked), and reaches the maximum when the density approaches zero (since there are no interactions). On the other hand, it is also reasonable that $V_0(\rho)$ might have a long tail in the high density regime, which may represent very rough grains or grains of nonuniform size. Hence, we have examined numerically the case with the following $V_0(\rho)$:

$$V_0(\rho) = \alpha/(1 + \beta\rho^2).$$

Our numerical results indicate that the direction of the convection rolls is quite different from the results obtained with a $V_0(\rho)$ that assumes a cutoff. Moreover, the four roll convection pattern appears when the long-tail $V_0(\rho)$ distribution is assumed. In Fig. 6 is plotted the convection streamline with $\alpha = 0.2$, $\beta = 0.5$. As we increase the vibrational frequency, the high intensity regime of the convection rolls moves toward the boundary. At some parameter regime, the two roll patterns evolve to four rolls. In Fig. 7, the four roll convection pattern is plotted.

In Figs. 6, 7, and 8 a wide parameter range has been examined. It seems that the appearance of the two roll pattern or four roll pattern depends not only on the aspect ratios, but also on the vibrational frequency and amplitude. Future work must focus on exploring the parameter space as well as the effect of boundary conditions to the convective patterns. We now present the linear stability analysis of the two-dimensional traffic equations.
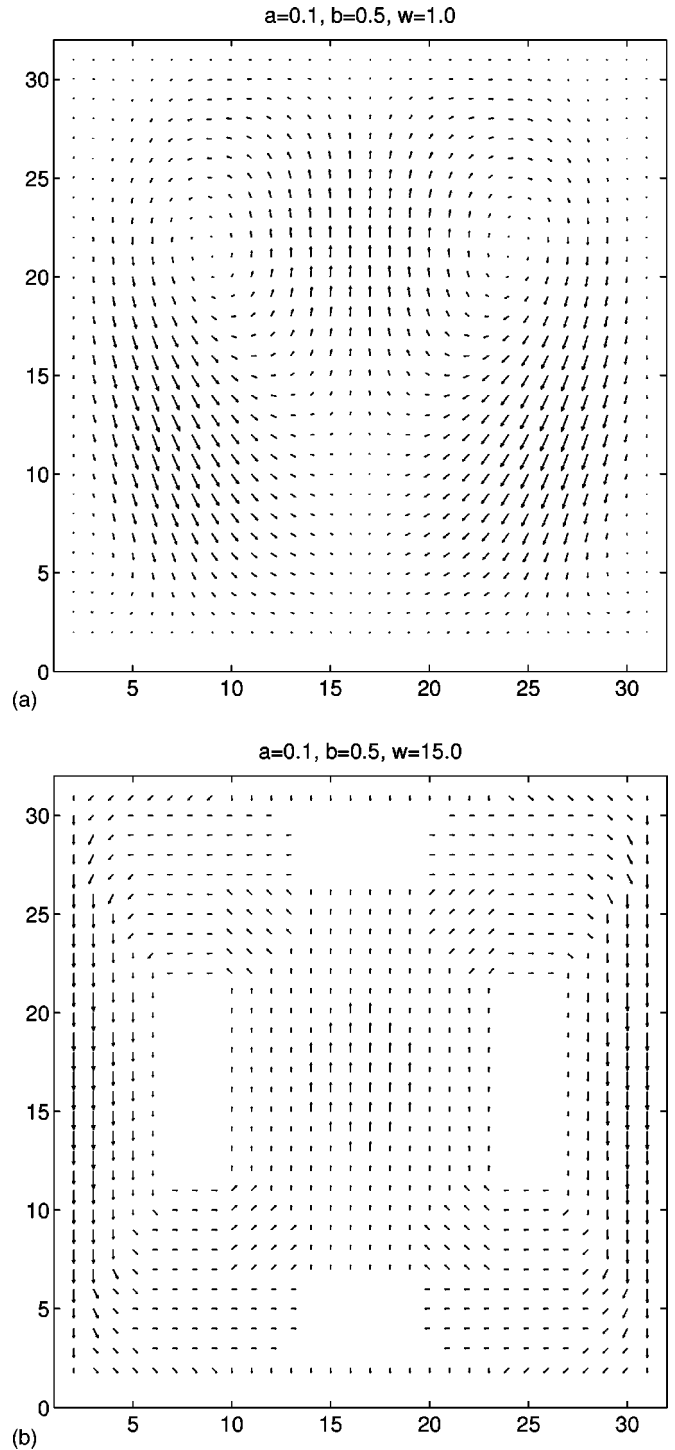

FIG. 6. Convection patterns for slow mean speed: For slow mean speed $\alpha = 0.1$, vibrating amplitude $A = 2.0$, $\beta = 0.5$. Two convection rolls appears for the different vibrating frequency, where higher frequency corresponds to a higher flow rate close to the boundaries, respectively, from left to right $\omega = 1.0$ (a) and $\omega = 15.0$ (b).

III. LINEAR STABILITY ANALYSIS OF TRAFFIC MODEL

Before studying the time-dependent properties of the vibrating beds, any model must make sure that the fixed bed solution, which is the ground state at $T = 0$ or equivalently $\Gamma = 0$ [23], must be stable.

a=0.5, b=0.5, w=1.0

a=5.1, b=0.5, w=1.0

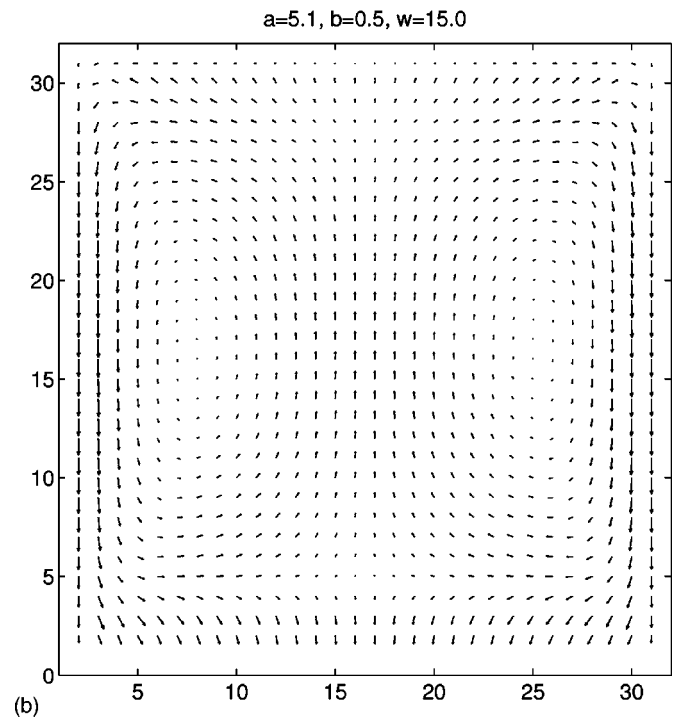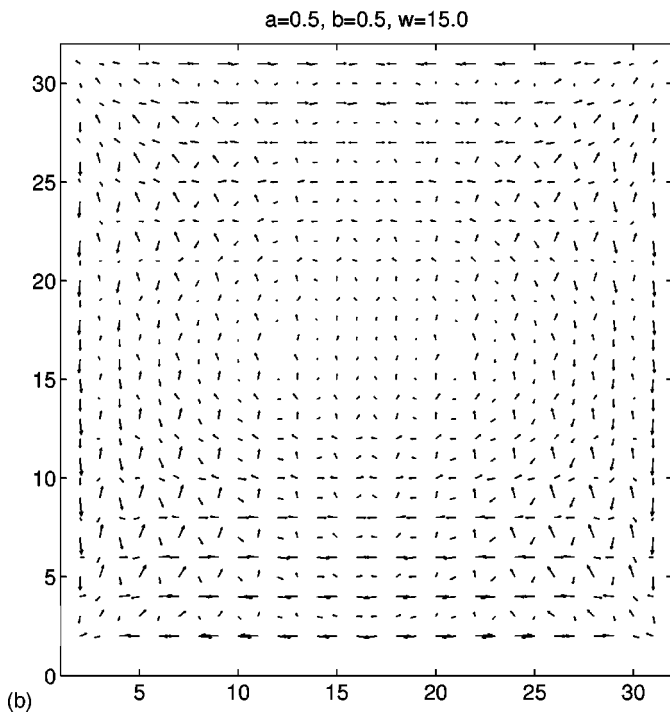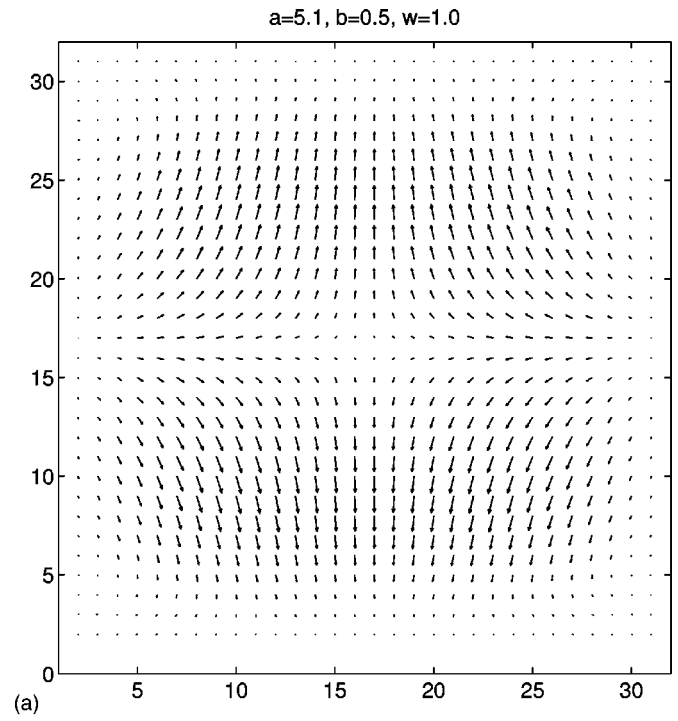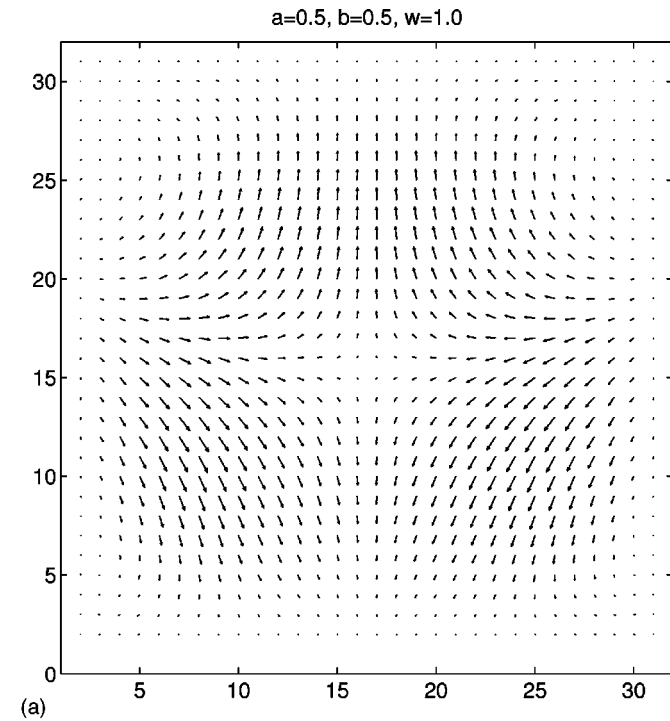a=0.5, b=0.5, w=15.0

a=5.1, b=0.5, w=15.0

FIG. 7. Convection pattern with four rolls: (a) Four convection roll appears when we increase the amplitude of the mean speed α = 0.5 with the frequency ω = 1.0. (b) As we increase the vibrating frequency, two roll convection patterns appear with a higher flow rate close to the boundaries.

FIG. 8. Convection pattern with four rolls: (a) Four convection roll persists when we increase the amplitude of the mean speed α = 5.1 with the frequency ω = 1.0. (b) As we increase the vibrating frequency, two roll convection pattern appears with a higher flow rate close to the boundaries.

A. Fixed bed solution

Equations (1)–(3) assume two different fixed bed solutions. The first one represents a uniform granular block characterized by the homogeneous density, $\rho = \rho_c$ such that $V(\rho_c) = 0$, and $\mathbf{v} = 0$. But there is a second *nonuniform* solution, given by Eq. (7). Both solutions represent fixed bed solutions. We only consider the stability of a uniform solu-

tion. Let $\rho = \rho_c + \rho_1$ and $\mathbf{v} = \mathbf{v_1}$. Substituting these into Eqs. (1)–(3), we find that ρ_1 satisfies the second order equation in time:

$$\ddot{\rho}_1 + \dot{\rho}_1/\tau - \mu\nabla^2\dot{\rho}_1 - T_e\nabla^2\rho_1 = 0. \qquad (8)$$

Assuming $\rho_1 = \rho_q(t)\sin(\hat{\pi}mx)e^{iqz}$, we find

$$\ddot{\rho}_q + B_0(q)\dot{\rho}_q + D_0(q)T_e\rho_q = 0 \qquad (9)$$

with

$$B_0(q) = 1/\tau + \mu(\hat{\pi}^2 m^2 + q^2), \qquad (10a)$$

$$D_0(q) = T_e(\hat{\pi}^2 m^2 + q^2). \qquad (10b)$$

For $\rho_q(t) \sim e^{\sigma t}$, it is straightforward to show that $\mathrm{Re}\,\sigma$ is always negative, i.e., $\mathrm{Re}\,\sigma < 0$. Thus, the uniform fixed bed solution is stable. For the stability analysis of a nonuniform solution, see Appendix B.

B. Stability of the bouncing solution

When the system is subjected to vibrations, how do uniform and nonuniform solutions evolve to eventually produce convective rolls? The standard way of proceeding in the stability analysis is first to find the basic solution, and then to examine its stability by performing the linear stability analysis of this basic solution. The onset of convection may be identified as a point at which such a basic solution becomes unstable. In the thermal convection problem such as the Rayleigh-Bénard convection, the basic solution is the laminar solution with a temperature-dependent density profile [25]. Since there exist two fixed bed solutions, we need to study the stability of these two solutions separately. In what follows, we present only the stability analysis associated with the uniform fixed bed solution, and show in Appendix B why the similar analysis for the nonuniform solution is nontrivial. Our analysis in what follows is based on the belief that since there is no difference between the two deep inside the bed, the mechanism for the convection for the uniform and nonuniform solutions might be the same. When $\Gamma \neq 0$, the basic solution associated with the uniform fixed bed solution is also a *homogeneous* solution in density, i.e., $\rho = \rho_0$, which then undergoes harmonic oscillations. This represents a uniform granular block, represented by a single ball [25], moving up and down bouncing at the plate. We previously termed such a solution a *bouncing solution* and such a bouncing solution can be readily found by inspection of the traffic equations (1)–(3). Its horizontal velocity is zero, but the vertical velocity $\omega_0(t)$ is given by

$$v_z = \omega_0(t) = -V_0(\rho_0) + \hat{V}(\rho_0,\tau,\Gamma)[\sin(\omega t) - \omega\tau\cos(\omega t)], \qquad (11)$$

where $\hat{V}(\rho_0,\tau,\Gamma) = \Gamma V_0(\rho_0)/(1 + \omega^2\tau^2)$. The numerically observed bouncing solutions in Fig. 2 may represent such a uniform bouncing solution.

We now examine the bouncing solution in some detail, which is essentially identical to a single ball dynamics, if we focus on the motion of the center of mass of the block. The dynamics of a ball on a vibrating plate is nontrivial for high vibration strength, but its trajectory obeys the simple Newtonian dynamics for low Γ with basically two characteristics: (i) the ball moves together with the plate for some time, (ii) the ball is launched to the space at a particular time t_0 that *depends* on the vibration strength. We assume that at the time of launching, the relative velocity between the block and the plate is such that the relative distance, $\Delta(t)$, between

the ball and the plate starts to increase at the time of launching. Hence, t_0 is determined by the condition

$$\frac{\Gamma}{1 + \omega^2\tau^2}[\sin(\omega t_0) - \omega\tau\cos(\omega t_0)] = 1 + \epsilon, \qquad (12)$$

where ϵ is determined by imposing the self-consistency $\Delta(t = t_0+) > 0$ [Eq. (14)]. Note that Eq. (12) ensures that

$$(1 + \epsilon + \omega^2\tau^2)^{1/2} \leq \Gamma. \qquad (13)$$

For Γ to be order one, τ needs to be of order $\sim 1/\omega$. Next, since the velocity is given, we find that the position of the ball in the moving frame, $\Delta(t) = \int_{t_0}^t \omega(t')dt'$, is given by

$$\Delta(t) = -V_0(\rho_0)(t - t_0) + \frac{\Gamma V_0}{1 + \omega^2\tau^2}$$
$$\times [\cos(\omega t_0) - \cos(\omega t)]/\omega - \tau(\sin(\omega t) - \sin(\omega t_0)]. \qquad (14)$$

In Fig. 9 are shown typical $v_z(t)$ and $\Delta(t)$ as a function of time. Note that Δ is the relative distance between the ball and the plate and thus cannot be negative: $\Delta(t)$ is positive for $t_0 \leq t \leq t_1$ where $\Delta(t_0) = 0$ and $\Delta(t_1) = 0$. $T_f = t_1 - t_0$, which is a function of the vibration strength Γ, is the flying time of the ball. For a set of parameters used in simulations, i.e., $\mu = \omega = \tau = 1.0$, and $V_0(\rho_0) = 0.5$, we find (t_0,t_1) changes from $(2.356,4.867)$ with $T_f = 2.51$ for $\Gamma = 2$ to $(1.197, 5.0368)$ with $T_f = 3.84$ for $\Gamma = 5$. For larger Γ, the flying time T_f obviously increases. Note that the relative velocity of the ball at the time of launching is not zero, i.e., $\omega(t_0) \neq 0$.

Let us now examine the stability of this bouncing solution. Let $\rho = \rho_0 + \rho_L$ and $\mathbf{v} = \omega_0(t)\hat{z} + \mathbf{v_L}$ and substitute ρ and v into Eqs. (1)–(3). Taking only the linear term, we find

$$\partial_t \rho_L + \rho_0 \nabla_\xi \cdot \mathbf{v_L} = 0, \qquad (15a)$$

$$\partial_t \mathbf{v_L} = \frac{T_e}{\rho_0}\nabla_\xi \rho_L - \frac{\mathbf{v_L}}{\tau} + \hat{z}\frac{V_0'(\rho_0)}{\tau}\rho_L[-1 + \Gamma\sin(\omega t)]$$
$$+ \mu\nabla^2 \mathbf{v_L}, \qquad (15b)$$

where $\xi = z - \int_0^t \omega(t')dt' \equiv z - \Delta(t)$. ξ measures the point of the granular block in the *box* frame that undergoes vibrations. Now, taking the divergence ∇_ξ of Eq. (15b) and substituting $\rho_0 \nabla_\xi \cdot v_L = -\partial_t \rho_L$, we find the equation for ρ_L:

$$(L_0 + L_1)\rho_L = 0, \qquad (16)$$

where

$$L_0 = \partial_t^2 - T_e\nabla_\xi^2 - \mu\nabla_\xi^2\partial_t, \qquad (17)$$

$$L_1 = \tau^{-1}\partial_t + \rho_0\tau^{-1}V_0'(\rho_0)[-1 + \Gamma\sin(\omega t)]\partial_\xi. \qquad (18)$$

In order to study the stability of the bouncing solution, we now seek a solution of the form

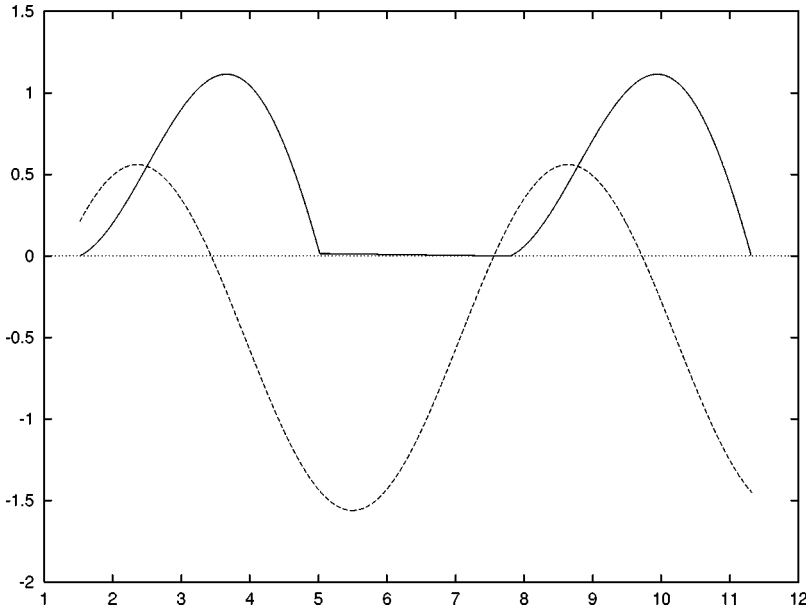$$\rho_L = \rho_{L,m,q}(t)\sin(\pi m x/L)e^{iq(\xi + \Delta)}. \qquad (19)$$

FIG. 9. Bouncing solutions. The velocity $\omega_0(t)$ (lower one), and the position (upper one) of the ball relative to the plate as a function of time. The ball is launched at $t=t_0$ [Eq. (14)] with a positive velocity $v_z(t_0)>0$, and flies in the air until it hits the plate again at $t=t_1$ with $\Delta(t_1)=0$. The ball stays at the plate and is relaunched at $t=t_0+2\pi/\omega$.

Note that m is an integer and $\xi+\Delta \equiv z$. Substituting Eq. (19) into Eq. (16), we obtain

$$\ddot{\rho}_q+B(q)\dot{\rho}_q+iC(q)\dot{\rho}_q+D(q)\rho_q+iE(q)\rho_q$$
$$=iL_q(t)\dot{\rho}_q(t)+M_q(t)\rho_q(t)+iN_q(t)\rho_q, \quad (20)$$

where

$$B(q)=B_0(q)=\mu(\hat{\pi}^2 m^2+q^2)+1/\tau, \quad (21a)$$

$$C(q)=-2qV_0(\rho_0), \quad (21b)$$

$$D(q)=D_0(q)-q^2\left(V_0^2(\rho_0)+\frac{\Gamma^2\hat{V}^2}{2}(1+\omega^2\tau^2)\right), \quad (21c)$$

$$E(q)=q\mu(\hat{\pi}^2+q^2)-\frac{\rho_0 q V_0(\rho_0)}{\tau}, \quad (21d)$$

$$L_q(t)=-2q\Gamma\hat{V}[\sin(\omega t)-\omega\tau\cos(\omega t)], \quad (21e)$$

$$M_q(t)=q^2\left[\frac{\omega^2\tau^2-1}{2}\Gamma^2\hat{V}^2\cos(2\omega t)-\omega\tau\Gamma^2\hat{V}^2\sin(2\omega t)\right], \quad (21f)$$

$$N_q(t)=-\Gamma\frac{\rho_0 q V_0'}{2}\sin(\omega t), \quad (21g)$$

where $\hat{\pi}=\pi/L$ with L the box size and $\rho_q(t)=\rho_{L,m,q}(t)$. For the most unstable mode, we set $m=1$. We now change the time, $t\to t_0+T$ and focus on the one oscillation from $T=0$ to $T=2\pi/\omega$. Then, Eqs. (21e)–(21g) are replaced by

$$L_q(t)\to-2q\Gamma\hat{V}\{[\sin(\omega t_0)-\omega\tau\cos(\omega t_0)]\cos(\omega T)$$
$$+[\cos(\omega t_0)+\omega\tau\sin(\omega t_0)]\sin(\omega T)\},$$

$$M_q(t)$$
$$\to q^2\Gamma^2\hat{V}^2\left[\left(\frac{\omega^2\tau^2-1}{2}\cos(2\omega t_0)-\omega\tau\sin(2\omega t_0)\right)\right.$$
$$\times\cos(2\omega T)-\left(\frac{\omega^2\tau^2-1}{2}\sin(2\omega t_0)+\omega\tau\cos(2\omega t_0)\right)$$
$$\left.\times\sin(2\omega T)\right],$$

$$N_q(t)\to-\frac{\Gamma\rho_0 q V_0'}{\tau}$$
$$\times[\sin(\omega t_0)\cos(\omega T)+\cos(\omega t_0)\sin(\omega T)].$$

The stability of Eq. (20) is highly nontrivial because it contains the time-dependent inhomogeneous term, and we employ here an approximation method that was first used in Ref. [8], namely, we replace the time-dependent function $L_q(T)$, $M_q(T)$, and $N_q(T)$ by their *average* over one period, namely, $\langle L_q(t)\rangle=T_f^{-1}\int_0^{T_f}dt L_q(T)$ with $T_f=(t_1-t_0)$, where the time-dependent parts in $L_q(t)$, $M_q(t)$, and $N_q(t)$ in Eq. (21) are replaced by their average values over the *flying* time:

$$\sin(n\omega T)\to\frac{1}{n\omega T_f}[1-\cos(n\omega T_f)],$$

$$\cos(n\omega T)\to\frac{1}{n\omega T_f}\sin(n\omega T_f),$$

where $n=1$ or 2. The validity of such an approximation may be justified since we are interested in the long-time behavior and the system continuously oscillates in time. Hence, we have replaced the *inhomogeneous* Eq. (20) into the *homogeneous* one:

$$\ddot{\rho}_q(T) + B(q)\dot{\rho}_q(T) + i\tilde{C}(q)\dot{\rho}_q(T) + \tilde{D}(q)\rho_q(T)$$

$$+ i\tilde{E}_q(T)\rho_q(T) = 0, \qquad (22)$$

where

$$\tilde{C}(q) = C(q) - \langle L_q(T)\rangle, \qquad (23a)$$

$$\tilde{D}(q) = D(q) - \langle M_q(T)\rangle, \qquad (23b)$$

$$\tilde{E}(q) = E(q) - \langle N_q(T)\rangle. \qquad (23c)$$

The stability of the homogeneous equation [Eq. (22)] with time-independent coefficients is easily determined by a standard linear stability analysis, namely, we set $\rho_q(t) = e^{\sigma t}$ and substitute this to Eq. (22) to obtain

$$\sigma^2 + [B(q) + i\tilde{C}(q)]\sigma + \tilde{D}(q) + i\tilde{E}(q) = 0. \qquad (24)$$

The condition for the instability is when the perturbations grow in time, i.e., Re$\sigma > 0$. Note that the solution of Eq. (24) is given by

$$\sigma_\pm = -\frac{B(q) + i\tilde{C}(q)}{2}$$

$$\pm \frac{1}{2}\sqrt{[B(q) + i\tilde{C}(q)]^2 - 4\tilde{D}(q) - 4i\tilde{E}(q)}. \qquad (25)$$

In order to extract the real part, we notice that the argument of the inside the square root may be written as $Re^{i\phi}$ with $R = [(B^2 - \tilde{C}^2 - 4\tilde{D})^2 + (2B\tilde{C} - 4\tilde{E})^2]^{1/2}$ and $\tan\phi = 2(B\tilde{C} - 2\tilde{E})/(B^2 - \tilde{C}^2 - 4\tilde{D})$. The real part of $\sigma_\pm$,

$$\text{Re}[\sigma_\pm] = -\frac{B}{2} \pm \sqrt{\frac{1}{2}\left[\sqrt{\left(\frac{B^2 - \tilde{C}^2}{4} - \tilde{D}\right)^2 + \left(\tilde{E} - \frac{1}{2}B\tilde{C}\right)^2} + \frac{B^2 - \tilde{C}^2}{4} - \tilde{D}\right]}. \qquad (26)$$

When the real part of Eq. (26) becomes positive, the bouncing solution becomes unstable. Hence, the instability condition for the most unstable branch becomes, Re$(\sigma_+) = -B/2 + R^{1/2}\cos(\phi/2) > 0$, which is rewritten by the following inequality:

$$(B\tilde{C} - 2\tilde{E})^2 \geq B^2(B^2 - |B^2 - \tilde{C}^2 - 4\tilde{D}|). \qquad (27)$$

Since the granular block is only in motion for the flying time, $0 \leq T \leq T_f$, but sits on the plate for $T_f < T < 2\pi/\omega$, the stability of the granular block needs to be determined by the *effective* instability condition, namely, for the flying time, Eq. (27) is operative, but for the rest of the time, the coefficients for the fixed bed solutions, (10a) and (10b), must be used. We thus define the effective instability condition:

$$\sigma_{\text{eff}} = T_f[(B\tilde{C} - 2\tilde{E})^2 - B^2(B^2 - |B^2 - \tilde{C}^2 - 4\tilde{D}|)$$

$$+ (2\pi/\omega - T_f) - B^2(B^2 - |B^2 - 4D_0|) > 0. \qquad (28)$$

When $\sigma_{\text{eff}} > 0$, the bouncing solution becomes unstable. Since $B(0) = \mu\hat{\pi}^2 + 1/\tau$, $\tilde{C}(0) = C(0) - \langle L_q(0)\rangle = 0$, $\tilde{D}(0) = D_0(0) - \langle M_q(0)\rangle = D_0(0) = T_e\hat{\pi}^2$, $\tilde{E}(0) = E(0) - \langle N_q(0)\rangle = 0$, we find $\sigma_{\text{eff}}(q=0) = -B(0)^2[B(0)^2 - |B^2(0) - 4D_0(0)|]2\pi/\omega$. If $B^2(0) > 4D_0(0)$ or $(\mu\hat{\pi}^2 + 1/\tau)^2 > 4T_e\hat{\pi}^2$, then $\sigma_{\text{eff}}(0) < 0$. If $B^2(0) < 4D_0(0)$, then $\sigma_{\text{eff}}(0) = 2B^2(0)[B^2(0) - 2D_0(0)]$ can be either positive or negative. If $\sigma_{\text{eff}}(0) > 0$, then the bouncing solution is always unstable. This determines the criterion for the existence of the bouncing solutions in the traffic equations: $(\mu\hat{\pi}^2 + 1/\tau)^2 < 4T_e\hat{\pi}^2$ and $(\mu\hat{\pi}^2 + 1/\tau)^2 > 2T_e\hat{\pi}^2$. And thus, if

$$(\mu + \hat{\pi}^2 + 1/\tau)^2 \leq 2T_e\hat{\pi}^2$$

then uniform bouncing solutions do not exist. Otherwise, we expect the bouncing solutions to appear.

In Fig. 10 is displayed σ_{eff} as a function of the wave number q for $\tau = \omega$, $\mu = 1$, $\rho_0 = 0.53$, $V_0(\rho_0) = 0.5$, $V_0'(\rho_0) = -10$, $L = 32$, and $T_e = 2.0$. Note that for $\Gamma < \Gamma_c$, $\sigma_{\text{eff}\,c}$ is always negative, and thus the bouncing solutions are stable. As we increase the control parameter Γ, the peak of σ_{eff} moves up and becomes zero at the critical $\Gamma_c = 2.27$, which signals the instability of the bouncing solutions, and thus is identified as the onset of convection. For $\Gamma > \Gamma_c$, there is a band of wave numbers where $\sigma_{\text{eff}} > 0$. The maximum growth rate is $q_c = 1.11$ for $\Gamma = 2.32$ and $q_c = 0.95$ at $\Gamma = 2.27$, which are of order one. The corresponding wave numbers for the convective rolls are $\lambda = 2\pi/k \sim 6$. Since there are two rolls in a box of size $L = 32$, the wavelength of the convective rolls is about 8, and our analysis is consistent with the numerical results. For other parameters, the qualitative feature is the same, namely, for $\Gamma < \Gamma_c$, $\sigma_{\text{eff}} < 0$ for all q, and at a critical Γ_c, the local maximum of σ_{eff} crosses zero at $q = q_c$, and for $\Gamma > \Gamma_c$, there is a band of wave numbers for which σ_{eff} is positive [24].

IV. DISCUSSION

We conclude this paper by briefly reviewing the present status of the convective instability of vibrating beds and simulations of the models presented here (model B) and elsewhere [1]. From our analytical as well as numerical analysis, we confirm that the bouncing motion of particle collections plays an important role in both model A and model B. We have, however, several issues that should be resolved in the near future.

First, we discuss the role of boundary conditions. We have employed no slip boundary conditions at the walls and the plate. Further, we have put the rigid walls at the top and
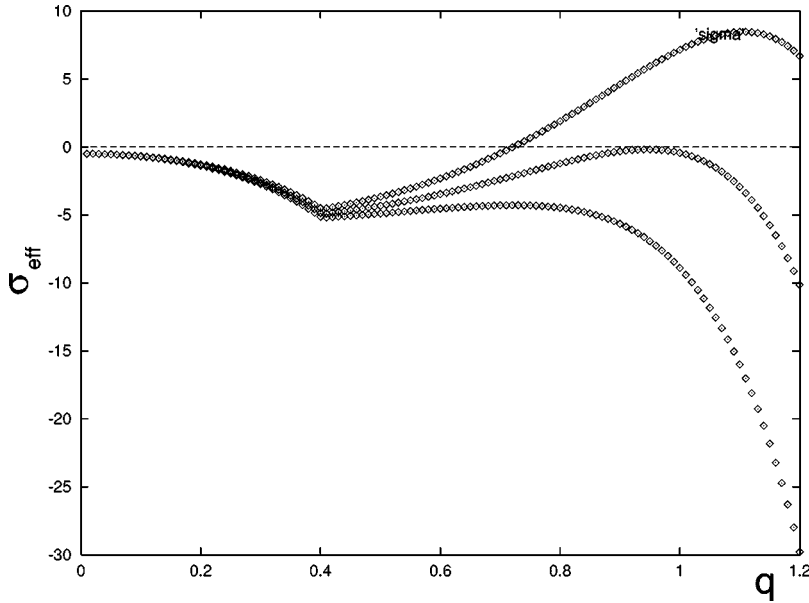
FIG. 10. The effective instability condition $\sigma_{\text{eff}}(q)$ (vertical axis) is plotted against the wave number q for different vibration strength Γ. At the critical $\Gamma_c = 2.27$, the local maximum of the growth rate crosses the zero. For $\Gamma = 2.2 < \Gamma_c$, $\sigma_{\text{eff}} < 0$ for all q, while for $\Gamma_c < \Gamma = 2.32$, there is a band of wave numbers for which $\sigma_{\text{eff}} > 0$.

thus suppressed the surface motion. Unlike the fluids, granular materials have been shown to exhibit very different motion near the wall in a zet flow experiment under gravity by Caram and Hong [20] and there has been some attempt to use the negative or positive slip to control the convective patterns [7]. Jenkins and Askari [31] derived slip boundary conditions at the wall based on the hydrodynamic equations derived from dissipative Enskog equation. However, more detailed studies on the boundary conditions at the wall are required.

Second, we discuss the role of interstitial fluid. The model A [8] assumes no interstitial fluid such as air, and it predicts a series of rolls for the vertically large aspect ratio. Model B on the other hand predicts that the convection suppresses in the bulk region but is confined near the surface, which appears to be in accordance with experiments and with the results of the two-fluid model with an interstitial fluid [26]. Perhaps, the origin of drag, or the relaxation term, whether it is coming from friction at the walls, or from the viscous effect of the interstitial fluid, or from long range correlations among voids, may not be relevant once it is present. However, the justification of its presence in the absence of interstitial fluid may require further studies, because it raises the validity of traffic equations at the conceptual level.

The suppression of the convection in the bulk is due to the locking mechanism of grains for near the closed packed density, which was taken into account in the present model B by a cutoff in $V(\rho)$, namely, $V(\rho) = 0$ for $\rho > \rho_c$. The results of model B, in particular the migration of convective rolls toward the surface (Fig. 4) and to the side walls (Fig. 5), seem to be more realistic and closer to the experimental and MD simulation results than those of model A. We certainly need more extensive studies of both model A and model B to make quantitative comparison with experiments.

Third, Knight et al. [32] studied the velocity profile of the grains in a vibrating bed and measured the dimensionless velocity profile, $\nu(\rho) \equiv v(z,r)/d$, where d is the particle diameter, and both r (the radius) and z (the vertical height) are measured from the center and $\rho = r/r_c$. They reported that

the velocity profile obtained by the following equation fits the experimental profile quite well:

$$\frac{d^2 \nu(\rho)}{d\rho^2} + \frac{1}{\rho}\frac{d\nu(\rho)}{d\rho} - \nu(\rho) = 0.$$

Note that the above equation appears to be consistent with the traffic equations at the closed packed density, where the relaxation function $V_0(\rho_c) = 0$ and the traffic equations (2) and (3), with the addition of the friction term, $-v_x/\tau$ in Eq. (2), reduce to the modified Darcy's law:

$$\mu \nabla^2 \mathbf{v} - \mathbf{v}/\tau = 0,$$

which is precisely the equation empirically obtained by Knight et al. It will be interesting to actually compare the velocity profile of the granular flows in other geometries such as the pipe flow, or a hopper flow with those predicted by the traffic equations, which in turn may enable one to identify and determine the parameters in the traffic equations. In this case, knowledge of the precise magnitude of the slip [20,31] at the wall is required.

Finally, future work must focus on completing the stability analysis for the spatially nonuniform solutions (Appendix B) and its instability mechanism along with the nonlinear analysis. In addition, the study of the surface instability and its connection to the surface fluidization and excitations as well as the study of horizontal vibrations and the onset of liquefaction [9,27] remain important open problems, which may shed insight into the oscillons [28] and other related surface instabilities [29]. Such studies are currently under way and will be reported in future communications.

ACKNOWLEDGMENTS

APPENDIX A: DERIVATION OF TRAFFIC EQUATION FROM ENSKOG EQUATION

We present here a brief derivation of the traffic equations from the Enskog equation. We first recall how one obtains the hydrodynamic equation from the Boltzmann equation [21]:

$$\frac{\partial f}{\partial t} + \mathbf{v} \cdot \nabla_r f + \mathbf{F} \cdot \nabla_v f = J_B, \tag{A1}$$

where F is the particle distribution function, and J_B is the collision integral. If χ is summation invariant, i.e., then $\chi_1 + \chi_2 = \chi_1' + \chi_2'$, where the prime refers to the velocities of the two colliding particles after the collision, and $\int d^3 p \chi(\mathbf{r}, \mathbf{p}) J_B = 0$. Now, one can derive hydrodynamic equations by multiplying $\int d^3 p \chi(\mathbf{r}, \mathbf{p})$ with Eq. (A1) as detailed in Huang [30]. We now just focus on the Navier-Stokes equation:

$$\left(\frac{\partial}{\partial t} + \mathbf{u} \cdot \nabla \right) \mathbf{u} = \mathbf{F}/m - \frac{1}{\rho} \nabla \left(P - \frac{\mu}{3} \nabla \cdot \mathbf{u} \right) + \frac{\mu}{\rho} \nabla^2 \mathbf{u}. \tag{A2}$$

For granular materials, we need to take into account two facts: first, particles are not point particles, but hard sphere particles with finite diameter D, so one should use the Enskog equation instead of the Boltzmann equation [21]. Second, we need to take into account gravity and friction, for which the external force term $\mathbf{F}$ in Eq. (A2) may be replaced by

$$\mathbf{F}/m = -g\hat{\mathbf{z}} - \gamma \mathbf{u}. \tag{A3}$$

The second term in Eq. (A3) is due to the friction. In the absence of interstitial fluid, its origin may lie in the frictions at the front and rear glass plates as well as at the walls, or in the long range correlations among voids. However, we point out that its presence in the absence of interstitial fluid needs more rigorous justification. Further, for the Enskog equation, there is collisional transfer. So, the pressure tensor has two components:

$$P_{ij} = P_{ij}^{\text{kinetic}} + P_{ij}^{\text{CT}}. \tag{A4}$$

The lowest order to the collisional transfer is $P_{zz} = \chi(\rho)\rho^2/2$ with $\chi = (1 - \rho/2)/(1 - \rho)^3$, where χ is the two particle equilibrium correlation function at the contact point of two colliding particles. It is known that the Enskog pressure has the following two components:

$$P = T\rho(1 + \chi\rho/2) = P_{\text{ideal}} + P_1. \tag{A5}$$

Let us focus only on the z component. Then, the Navier-Stokes equation becomes

$$\left(\frac{\partial}{\partial t} + u_z \frac{\partial}{\partial z} \right) u_z = -g - \gamma u_z - \frac{1}{\rho} \frac{d}{dz} P + (\text{viscous terms}). \tag{A6}$$

Now,

$$dP/dz = T[\rho' + \chi' \rho^2/2 + \rho\rho'\chi]$$

and the right-hand side of Eq. (A6) becomes

$$-g - \gamma u_z - \frac{1}{\rho} \frac{d}{dz} P + (\text{viscous terms})$$

$$= -g - \frac{T}{\rho} \frac{d\rho}{dz} - T(\chi'\rho/2 + \rho'\chi) - \gamma u_z$$

$$= -\frac{T}{\rho} \frac{d\rho}{dz} + \frac{[V(\rho) - u_z]}{\tau}, \tag{A7}$$

where $\tau = \gamma^{-1}$ and

$$V(\rho) = -\frac{T}{\gamma} [\beta + \chi'\rho/2 + \rho'\chi].$$

For a steady state $u_z = 0$, we find

$$\frac{T}{\rho} \frac{d\rho}{dz} = \frac{V(\rho)}{\tau} \tag{A8}$$

or equivalently

$$\rho'(1 + \rho\chi) + \rho\beta + \chi'\rho^2/2 = 0 \tag{A9}$$

with $\beta = g/T$. Hence, we have shown that the z component of the Navier-Stokes equation reduces to the traffic equation:

$$\left(\frac{\partial}{\partial t} + u_z \frac{\partial}{\partial z} \right) u_z = -\frac{T}{\rho} \frac{d\rho}{dz} + \frac{[V(\rho) - u_z]}{\tau} + \mu \nabla^2 u_z. \tag{A10}$$

For x and y components, we simply use the Boltzmann equation.

The actual form of $V(\rho)$ depends on χ, which is unknown. If we use the widely used form for χ [31] and demand self-consistency, then we find that the mean speed has the following form:

$$V(\rho) = -\frac{g}{\gamma} \frac{2(1 - \rho)^3 + 9/2 - 2\rho}{2(1 - \rho)^3}.$$

If we assume that the steady state is given by the Fermi distribution [23], then we find

$$V(\rho) = -\frac{g}{\gamma} \frac{4 - 17\rho + 8\rho^2}{4(1 - \rho)^2}.$$

In either case, the coefficient is proportional to the gravity. This is the reason for the functional form taken in Eq. (4) in the text. We caution that the functional form for $V(\rho)$ given above may not be taken too literally.

APPENDIX B: STABILITY ANALYSIS OF A SPATIALLY NONUNIFORM FIXED BED SOLUTION

We show here why the stability analysis of a spatially nonuniform fixed bed solution is complicated. In the absence of vibrations, $\Gamma = 0$, and the solution of this class, $\rho_0(z)$, is given by Eq. (7). Since the solution is spatially inhomogeneous, for small Γ, we seek bouncing solutions that are only a function of z:

$$\rho(z) = \rho_0(z) + \rho_0'(z)s(z)e^{i\omega t}, \qquad (B1)$$

$$v_z(z) = v(z)e^{i\omega t}, \qquad (B2)$$

where $\rho_0'(z) = d\rho_0(z)/dz$. We put Eqs. (B1) and (B2) into the traffic equations (1)–(3) and linearize to obtain

$$\frac{1}{\rho_0(z)}\frac{d\rho_0(z)}{dz}i\omega s(z) + \left(\frac{d}{dz} + \frac{1}{\rho_0}\frac{d\rho_0}{dz}\right)v(z) = 0, \quad (B3)$$

$$-c_0^2\frac{\rho_0'}{\rho_0}\frac{ds(z)}{dz} - i\omega v(z) - \left(1/\tau - \mu\frac{d^2}{dz^2}\right)v(z) = \frac{\Gamma}{\tau}V(\rho_0(z)). \qquad (B4)$$

Let $Q(z) = -(1/\rho_0)d\rho_0/dz = -1/\tau c_0^2 V(\rho_0)$. Then, we find equations for $Q(z)$ and $v(z)$:

$$-i\omega Q(z)s(z) + \left(\frac{d}{dz} - Q(z)\right)v(z) = 0, \qquad (B5)$$

$$-c_0^2 Q(z)\frac{ds(z)}{dz} + \left(i\omega + 1/\tau - \mu\frac{d^2}{dz^2}\right)v(z) = c_0^2\Gamma Q(z). \qquad (B6)$$

We need to find the solutions for Eqs. (B5) and (B6) that both satisfy the boundary conditions, $s(z), v(z) \to 0$ as $z \to \infty$, which appears to be nontrivial if we relax the condition that Γ is *not* a small parameter. Even though we are lucky to find the solutions, the stability analysis around these solutions still presents difficulties.

[1] A short version of this paper was published by H. Hayakawa and D. C. Hong, in *Powders and Grains 97*, edited by R. Behringer and J. Jenkins (Elsevier, New York, 1997), p. 417. See also e-print cond-mat/970396; Su. Yue, Ph.D. thesis, Lehigh University (1995).

[2] M. Faraday, Philos. Trans. R. Soc. London **52**, 299 (1831).

[3] For recent review see H. M. Jaeger, S. R. Nagel, and R. P. Behringer, Rev. Mod. Phys. **68**, 1259 (1996).

[4] P. Evesque and J. Rajchenbach, Phys. Rev. Lett. **62**, 44 (1989); C. Laroche, S. Douady, and S. Fauve, J. Phys. (Paris) **50**, 699 (1989); E. Clement, J. Duran, and J. Rajchenbach, *ibid.* **69**, 1189 (1992); J. Knight, H. Jaeger, and S. Nagle, *ibid.* **70**, 3728 (1993); H. Pak, E. van Doorn, and R. Behringer, *ibid.* **74**, 4643 (1995); E. E. Ehrichs, H. M. Jaeger, G. S. Karczmar, J. B. Knight, V. Y. Kuperman, and S. R. Nagel, Science **267**, 1632 (1995); H. Pak and R. Behringer, Nature (London) **371**, 231 (1994); K. Aoki, T. Akiyama, Y. Maki, and T. Watanabe, Phys. Rev. E **54**, 874 (1996).

[5] J. Gallas, H. Herrmann, and S. Sokolowski, Phys. Rev. Lett. **69**, 1371 (1992); Y-h. Taguchi, *ibid.* **69**, 1367 (1992).

[6] S. B. Savage, Adv. Appl. Mech. **24**, 289 (1984); P. Haff, J. Fluid Mech. **134**, 401 (1983).

[7] M. Bourzutschky and J. Miller, Phys. Rev. Lett. **74**, 221 (1995).

[8] H. Hayakawa, S. Yue, and D. C. Hong, Phys. Rev. Lett. **75**, 2328 (1995).

[9] T. Shinbrot, D. Khakhar, J. McCarthy, and J. M. Ottino, Phys. Rev. Lett. **79**, 829 (1997); K. Liffman, G. Metcalfe, and P. Cleary, *ibid.* **79**, 4574 (1997).

[10] For example, see C. S. Campbell, Annu. Rev. Fluid Mech. **22**, 57 (1990).

[11] G. W. Baxter, R. Behringer, T. Fagert, and G. Johnson, Phys. Rev. Lett. **62**, 2825 (1989).

[12] D. Helbing, *Verkehrsdynamik* (Springer, Berlin, 1997); I. Prigogine and R. Herman, *Kinetic Theory of Vehicular Traffic* (Elsevier, New York, 1971).

[13] B. S. Kerner and P. Konhauser, Phys. Rev. E **48**, R2335 (1993); **50**, 54 (1994); **51**, 6243 (1995); Phys. Rev. Lett. **79**, 4030 (1997).

[14] D. A. Kurtze and D. C. Hong, Phys. Rev. E **52**, 218 (1995).

[15] M. Bando *et al.*, Phys. Rev. E **51**, 1035 (1995).

[16] D. C. Hong, S. Yue, J. Rudra, M. Choi, Y. Kim, Phys. Rev. E **50**, 4123 (1994).

[17] O. Moriyama, N. Kuroiwa, M. Matsushita, and H. Hayakawa, Phys. Rev. Lett. **80**, 2833 (1998).

[18] H. Hayakawa and K. Nakanishi, e-print cond-mat/9802131.

[19] T. Hill and J. Kakalios, Phys. Rev. E **49**, 3610 (1994).

[20] H. Caram and D. C. Hong, Phys. Rev. Lett. **67**, 828 (1991); Mod. Phys. Lett. B **6**, 761 (1992); For earlier development, see J. Litwinyszyn, Bull. Acad. Polon. Sci., Ser. Sci. Tech. **11**, 61 (1963); W. W. Mullins, J. Appl. Phys. **43**, 665 (1972).

[21] For example, see S. Chapman and T. G. Cowling, *The Mathematical Theory of Non-uniform Gases* (Cambridge University Press, Cambridge, 1958); J. A. McLennan, *Introduction to Non-Equilibrium Statistical Mechanics* (Prentice-Hall, Englewood Cliffs, NJ, 1989).

[22] Y-h. Taguchi, Int. J. Mod. Phys. A **7**, 1839 (1993).

[23] H. Hayakawa and D. C. Hong, Phys. Rev. Lett. **78**, 2764 (1997).

[24] See, for example, P. Manneville, *Dissipative Structures and Weak Turbulence* (Academic Press, San Diego, 1990).

[25] For a single ball dynamics, see J. M. Luck and A. Mehta, Phys. Rev. E **48**, 3988 (1993), and references therein.

[26] H. Hayakawa and S. Sasa, Europhys. Lett. **17**, 685 (1992).

[27] S. Tennekoon and R. Behringer, patt-sol/9704001; D. E. Rosenkranz and T. Poschel, e-print cond-mat/9712108.

[28] F. Melo, P. B. Umbanhowar, and H. L. Swinney, Phys. Rev. Lett. **75**, 3838 (1995); Nature (London) **382**, 793 (1996); T. H. Metcalf, J. B. Knight, and H. M. Jaeger, Physica A **236**, 202 (1997); K. M. Aoki and T. Akiyama, Phys. Rev. Lett. **77**, 4166 (1996).

[29] J. Eggers and H. Riecke, patt-sol/9801004; L. Tsimring and I. Aranson, Phys. Rev. Lett. **79**, 213 (1997).

[30] K. Huang, *Statistical Mechanics* (John Wiley and Sons, New York, 1987), p. 96.

[31] J. T. Jenkins and E. Askari, *Powders and Grains 93*, edited by C. Thornton (Balkema, Roteerdam, 1993), p. 295.

[32] J. Knight, E. Ehrichs, V. Kuperman, J. Flint, H. Jaeger, and S. Nagel, Phys. Rev. E **54**, 5726 (1996).